THE AMERICAN SOCIETY OF MECHANICAL ENGINEERS
345 E. 47th St., New York, N.Y. 10017

95-GT-82

EXPERIMENTAL AND COMPUTATIONAL STUDY OF A RADIAL COMPRESSOR INLET

Jay M. Koch and Peter N. Chow
Turbo Products Division
Dresser-Rand
Olean, NY

Brad R. Hutchinson and Steve R. Elias
Advanced Scientific Computing
Waterloo, Ontario
Canada

ABSTRACT

Flow field measurements and flow visualization for a quarter scale model of a radial compressor inlet are presented for varying flow rates and inlet profiles. Non-uniform inlet profiles are created using a 90° bend directly upstream of the inlet. Experimental results are compared with the CFD analysis from a commercial 3-D Navier Stokes code. The experimental and computational results show good agreement, even in regions of reverse flow. The results from this study show CFD analysis can be used with confidence to predict the performance of radial compressor inlets.

NOMENCLATURE

P = Pressure, [psia]
M = Mach Number
LC = Total Pressure Loss Coefficient, $(P_{t_{01}}-P_{t_{03}})/(P_{t_{01}}-P_{s_{01}})$

Subscripts

s = static conditions
t = total conditions
01 = pipe inlet
02 = inlet flange
03 = guide vane exit
04 = downstream of guide vanes

INTRODUCTION

The use of radial inlets in industrial compressors is very common due to mechanical limitations which dictate the manner in which the flow can enter the machine. Although the radial inlet is widely used, the complex three dimensional flow in radial inlets is not well understood. Historically, simple guidelines have been used to determine the size and shape of the inlets, and losses were modeled with limited test data and empirical methods. To develop new inlet designs, model tests were used to determine the pressure drop across the inlet and the characteristics of the inlet flow field. The primary tool available to study the complex 3-D flow field was flow visualization using tufts or smoke. Developing inlets in this manner is iterative in nature and thus time consuming and expensive. It is also difficult to determine the influence of different geometric variations, due to the small pressure drop in the inlet, limited instrumentation, and limitations of the flow visualization techniques.

Besides constraints due to manufacturing, other factors that affect the design of compressor inlets are available space and inlet piping. The recent trend in compressor manufacture is to have equivalent compressor performance in smaller packages. The result is less available space for the inlet. Customer installations can also have a large effect on the inlet performance due to piping arrangements which result in a bend or series of bends in close proximity to the compressor inlet. Field experience has shown that these types of installations can have adverse affects on the compressor performance.

Recently, Computational Fluid Dynamics (CFD) has been used to evaluate and successfully modify a pipeline booster inlet design (Flathers et al., 1994). That design used complex shapes to achieve the desired loss levels, pressure profiles and exit flow angle distributions. However, it is often desirable for manufacturing reasons to make the inlet shape as simple as possible, especially for applications where the production quantities are limited and casting is not economically feasible. Unfortunately, the side effects of simple geometry are less than optimum performance, such as regions of separation, and higher loss levels. The recent paper by Flathers et al. (1994) shows good comparison between CFD and experiment for well behaved

Presented at the International Gas Turbine and Aeroengine Congress and Exposition
Houston, Texas - June 5-8, 1995

flow, but CFD results for radial inlets with regions of separated flow are not available in the open literature. This paper presents CFD and experimental results for simpler inlet geometries, where the flow is more non-uniform than previously reported.

In order to enhance the understanding of radial inlet flows, a project was undertaken wherein a radial inlet was studied both experimentally and using CFD. The inlet evaluated was compact, used simple shapes, was easily fabricated and was designed using historical methods. Other goals of the project were to verify the application of CFD to inlets of this type, so CFD could be used with confidence in the design process, and to determine the impact of different operating conditions and inlet piping configurations on the inlet performance. It is hoped that this knowledge will permit confident, rapid design of efficient inlets, of the type that are subject to manufacturing and space constraints, and that these inlets will be more robust for a wide range of inlet configurations.

COMPUTATIONAL METHODS

The majority of this paper is concerned with presenting the numerical and experimental findings of a radial compressor inlet study. It is therefore important that some description of these methods are provided to assist in the evaluation of presented results. The computational approach is discussed here, and the experimental methods are presented later.

The numerical investigation consisted of a fully three-dimensional Navier-Stokes analysis of the inlet, using the commercially available code TASCflow. TASCflow uses a finite-volume method to solve the primitive variable, Reynolds-averaged form of the Navier-Stokes equations. As it employs a pressure based formulation, it is applicable to both fully incompressible and compressible (subsonic, transonic, and supersonic) flows. This is an important consideration for the current study, since considerable Mach number variation is observed, and regions of very low Mach number (hence almost incompressible) flow are present. The method is fully conservative, meaning that fluxes of all modeled quantities are preserved both locally and globally.

The discretization method and physical models employed by a CFD code impacts the accuracy of the computed flow field. In this investigation, the analysis region is sub-divided into hexahedral elements. The finite volumes, which are the regions over which the principles of conservation are enforced, are formed from the elements (Advanced Scientific Computing, 1994). The advantage of this procedure is that the number of flux evaluations per face is four, instead of one, thereby yielding higher accuracy for a given mesh size. Hexahedral (as opposed to tetrahedral) elements are used because they are well suited to the high cell aspect ratios (a cell is much longer parallel to the wall than in the direction normal to the wall) that naturally results from attempting to resolve the near wall regions, because of their inherent accuracy and economy, and because they are relatively less sensitive to mesh skewness.

TASCflow uses a physically-based second order spatial discretization method that is comprised of two main components. The first component provides the directional sensitivity and is known as Linear Profile Skew upwinding. The second component insures appropriate variation of stagnation conditions, and is known as Physical Advection Correction (Galpin et al., 1986, and Van Doormaal et al., 1987). The net result is a second order scheme which exhibits low levels of discretization error on a course mesh, an important property for the present study. Other important algorithms include the turbulence model and the pressure-velocity coupling treatment. The standard k-e turbulence model with wall functions accounts for the effects of turbulent transport. A fourth-order pressure redistribution which is standard for pressure-based (as opposed to density-based, time marching) methods is employed to prevent pressure-velocity decoupling for low Mach number flows.

The geometric complexity of radial compressor inlets requires that meshes of substantial size be used, so an important consideration is computational efficiency. TASCflow uses a coupled iterative solution method which is accelerated by the Additive Correction Multigrid scheme (Hutchinson and Raithby, 1986, Raw, 1994). This method yields rapid convergence for a wide range of problems, can tolerate a wide range of size and shapes of control volumes and the solution cost is linearly proportional to the number of mesh nodes.

Another feature important to the analysis of radial inlets is the availability of a wide range of boundary conditions. Choices for inlet boundary conditions include velocity, mass flow or total pressure and direction specification (in addition, static or total temperature and turbulence quantities must be specified). At the exit, it is possible to set the static pressure (at one location, or over the entire boundary) or the mass flow.

COMPUTATIONAL STUDY

The inlet used for computational study is a quarter scale model. The inlet consists of a nozzle connected to a constant area plenum followed by radial guide vanes at the exit of the plenum. Splitter vanes are located in the nozzle, at top dead center, 0°, (TDC) in the plenum, and at bottom dead center, 180° (BDC) in the plenum. There are eight radial guide vanes, all equally spaced. Three different piping arrangements, all shown in Figure 1, were studied. These were: A) a straight pipe, B) a 90° short radius elbow, with elbow centerline perpendicular to compressor axis, and C) a 90° short radius elbow, centerline aligned with compressor axis. The inlet for each configuration was a straight pipe two flange diameters in length. For configuration A this pipe was attached directly to the nozzle flange. For configurations B & C this straight pipe was attached to the elbow, with the elbow being directly attached to the nozzle flange.

For configurations A & C, a 180° model could be used with a symmetry plane along the center of the inlet. Configuration B required a full 360° model, due to the asymmetric inlet conditions. The complete grid for the full geometry was constructed by first creating sub-grids for the pipe/elbow section, nozzle section, plenum section, and radial guide vane section. The complete mesh was then formed by joining the sub-grids using the "grid attaching" feature of the software. All sections other than the pipe/elbow sections were 180° sections which

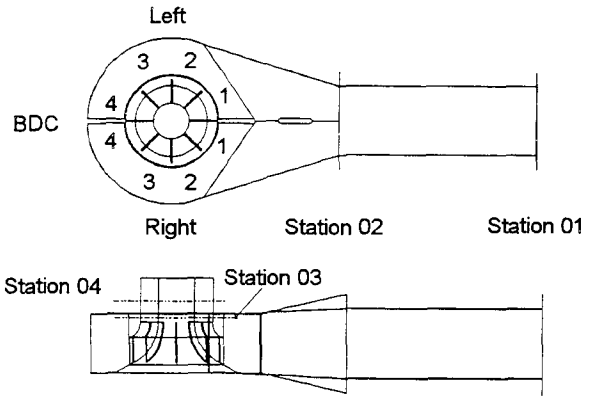

FIGURE 1A. CONFIGURATION A

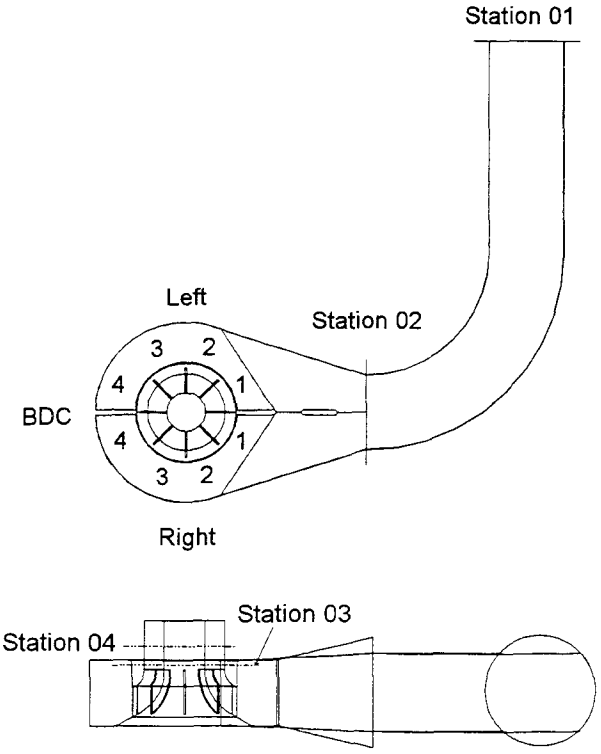

FIGURE 1B. CONFIGURATION B

were mirrored to create a 360° model. A straight extension was added to the exit of radial guide vanes to prevent biasing the flow code results by having the grid exit being too close to the area of interest, i.e. the area just downstream of the radial guide vanes.

In order to determine sensitivity of the computed solution to the mesh size, a series of runs with increasing mesh size were performed on the 180° model of configuration A. The final mesh was limited to approximately 250,000 nodes due to memory limitations, therefore the largest 180° model was limited to

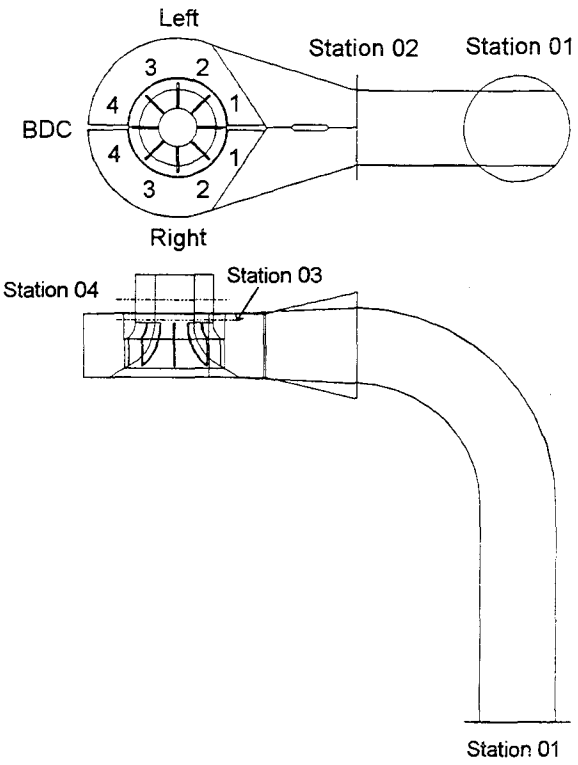

FIGURE 1C. CONFIGURATION C

approximately 125,000 nodes. As grid size increased a rise in the predicted total and static pressure was noted. This result indicates that the coarser meshes were insufficient to resolve the flow, and numerical errors were manifested as a loss in total pressure. In addition, the solution was found to be more sensitive to an increase of nodes in the streamwise direction than in the circumferential direction. The rate of change of various mass averaged flow quantities at the system exit (total pressure, static pressure) was observed to decrease with mesh refinement, however small differences (0.1% of the inlet total pressure) were still observed between the second finest and finest meshes. This result indicates that the finest mesh is not quite sufficient to provide a grid independent numerical flow prediction, and hence for this and other modeling reasons, some variation with experimental data should be expected. The final 360° mesh, shown in Figures 2 & 3, was 254,208 nodes for all configurations.

The inlet stagnation conditions for the problem were set to atmospheric pressure and room temperature, with a uniform profile (to match the intended experimental test conditions). The mass flow for the problem was specified at the exit of the system, and was set to give a specific Mach number at the inlet of the straight pipe. All calculations were made using hydraulically smooth walls. Starting from a uniform initial guess, the flow code required approximately 130 iterations to converge to a RMS residual of 1e-6 (maximum residual of 1e-4). The approximate computational time required for the solution was 29 hours on a IBM RS/6000 Model 590. For the 180°

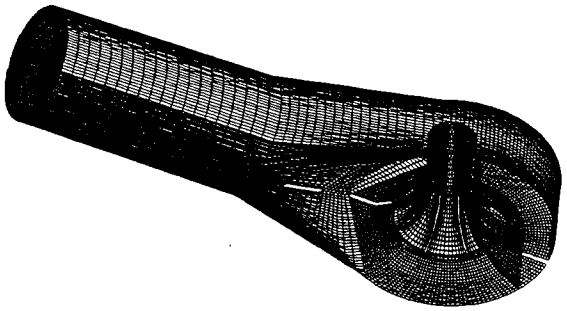

FIGURE 2. FINAL GRID

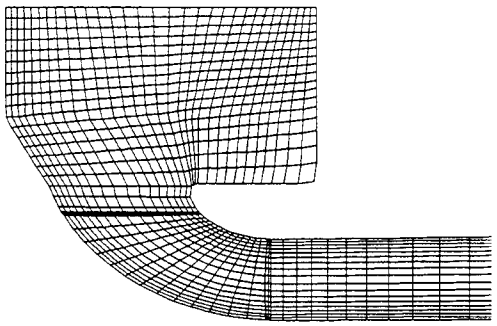

FIGURE 3. RADIAL GRID SECTION

model (127,104 nodes), the approximate computational time was 14 hours.

COMPUTATIONAL RESULTS

To ensure that the symmetry boundary condition worked properly, the 180° model used for grid sizing was compared to the 360° model for configuration A. This comparison is important because it is preferable to use the 180° model for design work, allowing reduced grid size and computation time. As expected, the 180° model matched the 360° model. The only variations which were evident were very small variations in the Mach number in the low Mach number regions of the plenum near BDC.

After reviewing the symmetry condition, the general trends in the inlet were reviewed for the inlet design Mach number of 0.13. For this operating condition, recirculation regions exist in several areas: in the plenum at TDC over the flat portion of the shroud wall, in the bottom of the plenum near the splitter vane, and at the radial guide vane exit. These flow features are shown in Figures 4 and 5. Figure 6 is a mid-span cut through the plenum and guide vane sections of the inlet (both sides of the inlet are shown). This figure indicates significant circumferential flow angle variation at the entrance of the guide vane section. The flow is nearly radial at TDC, nearly tangential at 90°, and again near radial at BDC. The trend of varying flow angle with circumferential location was also noted by Flathers et al. (1994), but the largest flow angle reported was approximately

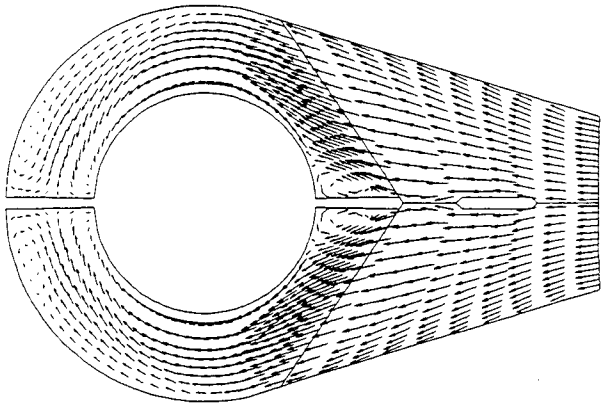

FIGURE 4. PLENUM SECTION VELOCITY VECTORS CONFIGURATION A

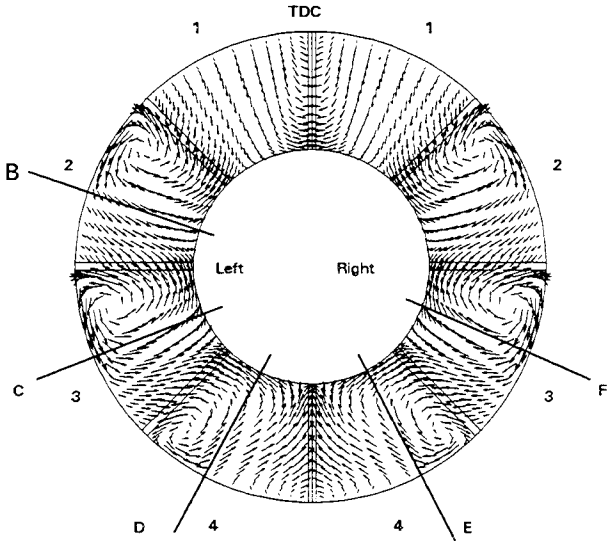

FIGURE 5. GUIDE VANE TRAILING EDGE VELOCITY VECTORS – CONFIGURATION A

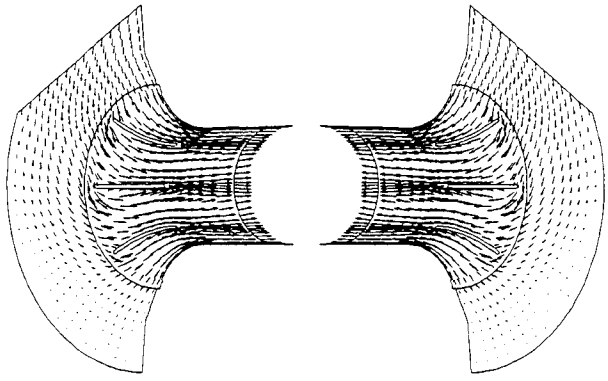

FIGURE 6. GUIDE VANE MID-SPAN VELOCITY VECTORS – CONFIGURATION A

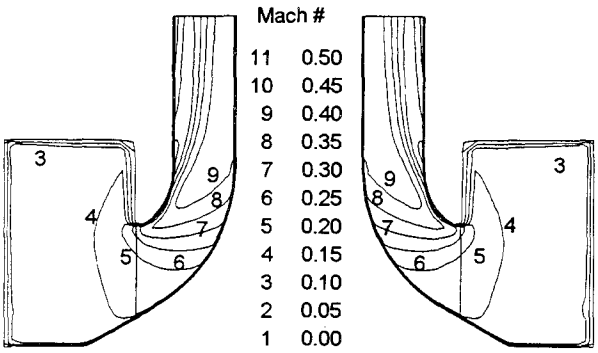

FIGURE 7. PASSAGE 2 MACH NUMBER CONFIGURATION A

TABLE 1. MASS AVERAGES - CONFIGURATION A

Pipe Inlet (01)			Left Side (03)			Right Side (03)		
Mach#	Pt	Ps	Pt	Ps	LC	Pt	Ps	LC
0.08	14.699	14.635	14.562	14.038	2.14	14.562	14.037	2.14
0.13	14.699	14.529	14.331	12.842	2.16	14.331	12.842	2.16
0.19	14.699	14.339	13.837	9.694	2.39	13.839	9.692	2.39

TABLE 2. MASS AVERAGES - CONFIGURATION B

Pipe Inlet (01)			Left Side (03)			Right Side (03)		
Mach#	Pt	Ps	Pt	Ps	LC	Pt	Ps	LC
0.13	14.699	14.527	14.296	12.829	2.34	14.307	12.819	2.28
0.19	14.699	14.339	13.766	9.644	2.59	13.790	9.694	2.52

TABLE 3. MASS AVERAGES - CONFIGURATION C

Pipe Inlet (01)			Left Side (03)			Right Side (03)		
Mach#	Pt	Ps	Pt	Ps	LC	Pt	Ps	LC
0.13	14.699	14.529	14.319	12.846	2.24	14.319	12.846	2.24
0.19	14.699	14.338	13.803	9.697	2.48	13.803	9.696	2.48

40°, which is much less than the predicted results for the inlet of this study. Additionally, it can be seen from the low Mach numbers in the bottom of the plenum that the area in that region is too large.

The region of separation in the plenum over the flat portion of the shroud wall appears to be due to the flow not being able to transition the tight curvature required to adjust from the radial inflow to the tangential movement around the inlet. The flow which exits the nozzle at TDC encounters a pressure gradient, which performs the dual functions of turning the flow from the radial direction to the tangential direction, and also turning the flow axially (from the shroud towards mid-span). The separation region is a consequence of the sharp geometric turn, and associated large local pressure gradient. The separation region in the bottom of the plenum is due to a similar phenomenon. Figure 6 indicates that the regions of separation at the inlet to the radial guide vanes are due to high incidence angles. Also evident, in Figure 7 is the rapid acceleration along the shroud wall as the flow exits the plenum and enters the radial guide vanes. The figure shows the mid-passage conditions for the second vane passage for each side of the inlet (left and right).

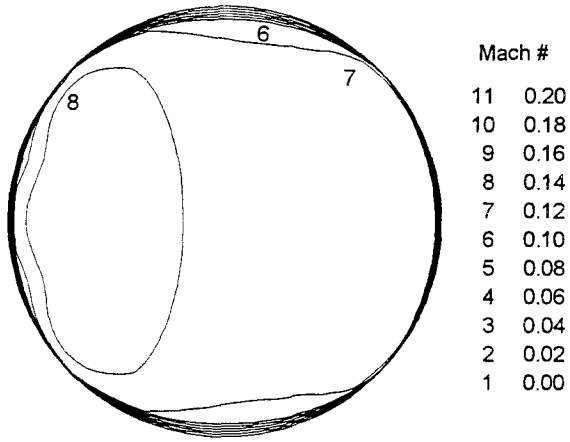

FIGURE 8. ELBOW EXIT MACH NUMBER CONFIGURATION B

Comparisons of the Mach number = 0.13 case to the other Mach number cases reveals that the general flow patterns in the inlet are independent of Mach number, but that the magnitudes of the patterns (Mach number, velocities and pressures) are dependent on the Mach number. Thus the flow angle is nearly constant for all Mach numbers.

Mass averaging the results reveals that the total pressure loss coefficient, LC, varies with Mach number, and that the losses increase significantly at higher Mach numbers. The mass averaging also verified that the flow is evenly distributed in the four radial guide vane passages on each side of the inlet. Table 1 shows the mass averaged total pressure, static pressure, and the loss coefficient.

The overall results for configuration B are very similar to configuration A and only small changes were noticed in the guide vane exit profiles. The mass averaged values in Table 2 further support the observed flow similarity. The results for configuration B reveal a region of higher velocity on the inner wall of the elbow that covers 40% of the upstream elbow exit area (Refer to Figure 8). This high velocity region moves into the nozzle and then into the left side of the plenum where it slowly mixes out. Figures 9A-D show Mach number on meridional cuts through the mid-planes of the radial guide vane passages. Each figure indicates that the flow is generally quite similar in the two sides of the inlet, although small differences do exist. Other noticeable features are the reduction in the bulk flow speed in the plenum, the rapid acceleration and curvature around the shroud wall and the overall general similarity of flow patterns in each of the guide vane passages. Figure 10 indicates that the near-shroud flow in the plenum is similar to that observed for configuration A (shown in Figure 4), except for three distinct features. First, the flow is biased to the left side of the plenum due to the effect of the upstream elbow. Second, the flow at BDC is slightly different in that the primary tangential flow does not reach BDC, and the previously observed re-circulation pattern is not present. It appears that the BDC region receives its flow from another axial position, instead of tangentially. Third, a swirl cell is observed at about the 135° position on the left side of the plenum. This stall cell extends

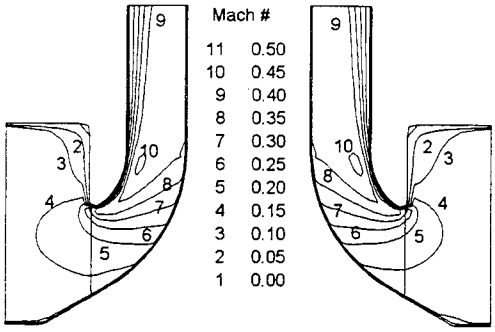

FIGURE 9A. PASSAGE 1 MACH NUMBER CONFIGURATION B

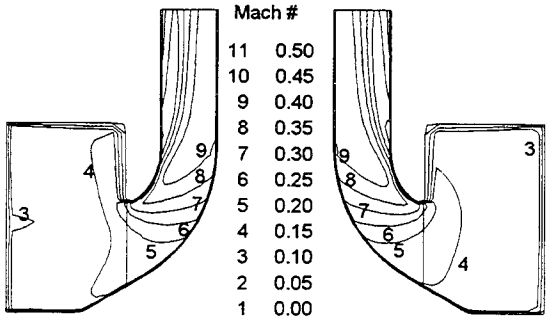

FIGURE 9B. PASSAGE 2 MACH NUMBER CONFIGURATION B

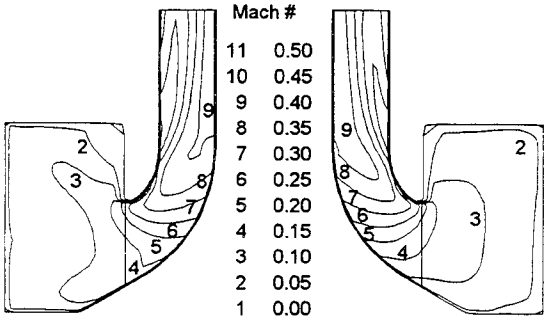

FIGURE 9D. PASSAGE 3 MACH NUMBER CONFIGURATION B

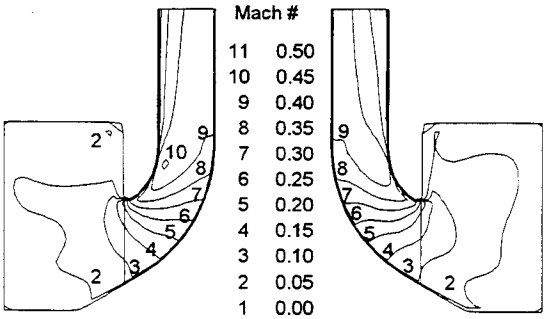

FIGURE 9D. PASSAGE 4 MACH NUMBER CONFIGURATION B

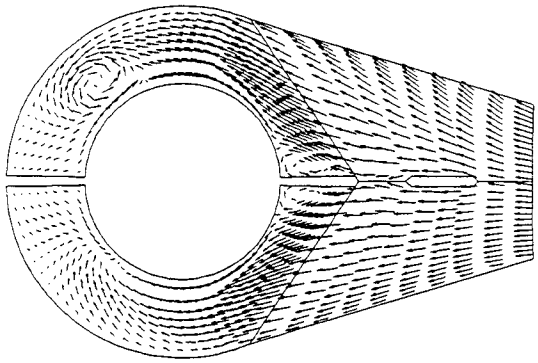

FIGURE 10. PLENUM SECTION VELOCITY VECTORS CONFIGURATION B

from the plenum shroud wall to the shroud wall of the radial guide vane inlet.

The overall results for configuration C are very similar to configuration A and only small changes can be seen in the guide vane exit profiles and mass averaged values (Refer to Table 3). Figure 11 shows that the flow exiting the upstream elbow is asymmetric, with a region of high velocity extending from the inner wall of the elbow to the center of the pipe. This high velocity region moves into the nozzle and is then split as it moves into the two sides of the plenum where it slowly mixes out. Because the region of high velocity is evenly distributed between both sides of the plenum, the results for both sides of the plenum are very similar. The separation zones in the bottom of the plenum are very similar to the separation zone for the right side of configuration B, and are much smaller than the separation zones for configuration A. (Refer to Figures 4, 10, & 12) It seems that, particularly for configuration C, the higher momentum hub flow exits the upstream elbow, passes through the nozzle and plenum, and then travels in an axial direction up the plenum wall, providing flow to the BDC shroud region.

The results for all three configurations show that the losses in the inlet are a function of Mach number squared but the general flow patterns in the inlet are independent of Mach number. The results also show that the distortion from the elbow is mixed out in the plenum. The addition of the elbow does increase the losses slightly and changes the flow characteristics in the bottom of the plenum, but it does very little to change the exit profile of the inlet. The study does however, reveal several locations where design modifications could improve the performance of the inlet, i.e. separation regions in the plenum, high velocities along the shroud, and separation regions due to high incidence on the guide vanes.

EXPERIMENTAL STUDY

The model used for the experimental study is the same quarter scale model used for computational study (Refer to Figure 1A-C). A diagram of the model is shown in Figure 13. The pipes, flanges, and elbows used for the model were commercially available piping. The nozzle was manufactured from sections of Styrofoam which were glued together. The portion of the nozzle sections exposed to the flow was sealed and sanded to provide a

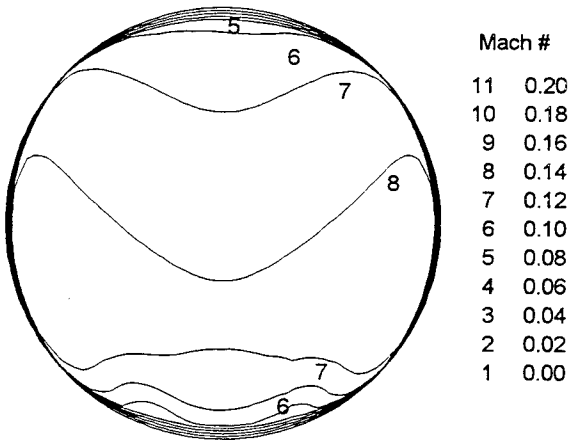

FIGURE 11. ELBOW EXIT MACH NUMBER CONFIGURATION C

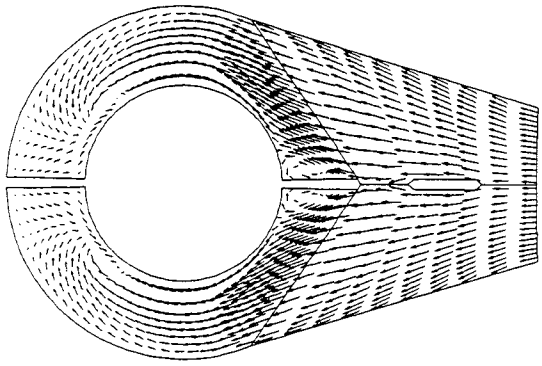

FIGURE 12. PLENUM SECTION VELOCITY VECTORS CONFIGURATION C

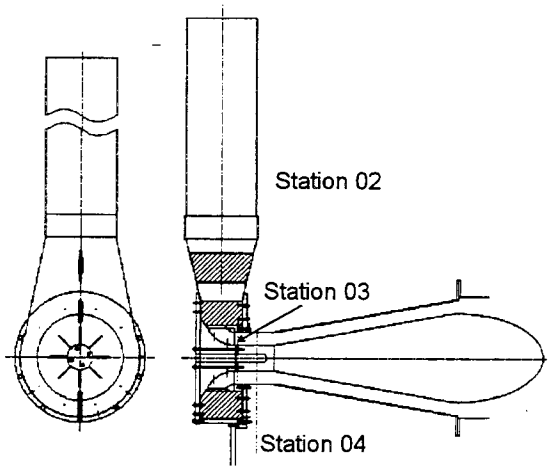

FIGURE 13. SCALE MODEL DIAGRAM

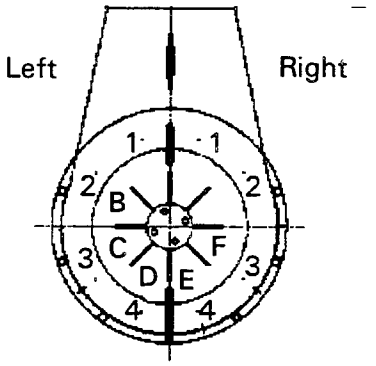

FIGURE 14. TRAVERSE PROBE LOCATIONS

smooth surface. The inlet plenum was fabricated from Lexan to allow flow visualization. The guide vane hub wall was fabricated from birch wood but the guide vane shroud wall and the radial guide vanes were manufactured from aluminum. A straight extension three guide vane exit passage widths in length followed the guide vanes. An annular diffuser was attached to the extension to provide sufficient pressure recovery to operate the model at the maximum flow rate. Flow was drawn through the model using a blower powered by a 75 hp electric motor. The piping connecting the model to the blower was isolated with a rubber coupling and was heavily sandbagged to damp any oscillations from the blower.

Instrumentation consisted of wall static taps, thermocouples, and traverse probes. Two static taps were located just downstream of the inlet bellmouth to determine the inlet Mach number (Station 01). At the inlet flange (Station 02) the wall static pressure was measured using three static taps, and the inlet total temperature was measured using two thermocouples. Measurements across the passage were made using a traverse probe at 0°, moving perpendicular to the compressor axis. The guide vane exit (Station 03, 0.5 guide vane passage widths downstream of guide vanes) conditions were measured using four equally spaced static taps on the hub and shroud walls. The guide vane downstream (Station 04, 1.5 guide vane passage widths downstream of guide vanes) conditions were measured using radial traverse probes at five circumferential locations. Twenty-six additional static pressure taps were located on the plenum walls.

Temperatures were measured using half-shielded Type E (chromel - constantan) thermocouples. The overall accuracy of the thermocouple measurements (RMS) was +/- 0.201 °R. Pressures were measured using Validyne variable reluctance pressure transducers. Two transducers were used to measure model pressures, a low pressure transducer, and a high pressure transducer. The overall accuracy (RMS error) of the low pressure transducer was +/- 0.007 psi. The overall accuracy (RMS error) of the high pressure transducer was +/- 0.016 psi. Water manometers were used to continuously monitor transducer accuracy during testing.

All traverses used 3 hole cobra probes to measure total pressure, static pressure and flow angle. The flow angle was determined by balancing the two side tube pressures. The 3 hole cobra probes were calibrated in a wind tunnel with a pressure accuracy (RMS error) of +/- 0.014 psi and an angle accuracy of approximately +/- 0.5 degrees.

Test Procedure

The flow through the inlet was controlled using a valve located downstream of the radial inlet model, near the blower inlet. The pipe inlet Mach number was calculated using atmospheric pressure (stagnation pressure) and the inlet static pressure measured down stream of the inlet bellmouth (Station 01). The Mach number was calculated for compressible, isentropic flow using equation 1.

$$\frac{P_t}{P_s} = \left[1 + \frac{\gamma - 1}{2} M^2\right]^{\frac{\gamma}{\gamma - 1}} \qquad (1)$$

Configuration A was tested at three Mach numbers (0.08, 0.13, 0.19), and configurations B & C were tested at two Mach numbers (0.13, 0.19). Traverse measurements were made for each operating condition tested. Inlet flange traverse measurements were made at 5%, 15%, 25%, 35%, 45%, 55%, 65%, 75%, 85%, and 95% passage width, with 0% being closest to the left side of the plenum wall and 100% being closest to the right side of the plenum wall. The guide vane downstream traverse probes were located at circumferential angles of 72°, 108°, 144°, 216°, and 252° (labeled B-F respectively in Figure 14) with 0° being TDC, 180° BDC, moving clockwise, forward looking aft. The guide vane traverses were made at 1.2%, 12.3%, 23.3%, 34.4%, 45.5%, 56.6%, 67.7%, 78.8%, 89.8%, and 98.8% guide vane passage width, with 0% being the hub wall and 100% the shroud wall.

For flow visualization, small tufts were placed in the inlet pipe, on the nozzle splitter vane, on the plenum splitter vanes, on the walls of the plenum, and on the inlet guide vanes.

COMPARISON OF COMPUTATIONAL AND EXPERIMENTAL RESULTS

The format for the comparison of computational and experimental results will be plots of total pressure, static pressure, and flow angle for three different traverse locations downstream of the guide vanes. The total pressure and static pressure have been normalized by the inlet total pressure. Traverse locations at 108°/252° (C/F) and 144°/216° (D/E) represent the same circumferential location on different sides of the inlet, and will therefore be shown together to compare symmetry effects.

The data comparison for configuration A is shown in Figures 15-17. Overall, the data agrees very well. The differences between the experimental pressures and the calculated pressures are within 1-2% of the pipe inlet total pressure. This is similar to the findings of Flathers et al (1994). The agreement is good despite the regions of separated flow in the guide vane passages which are still evident at the measurement plane. The total pressure however, is slightly over predicted in these regions of separation. The trend in the calculated static pressure is correct, but the level is slightly low. The largest discrepancy is in the comparison of flow angle, where there are differences of up to 20°. The computed flow angles follow the same trends as the experimental data, but the extreme variations are not captured. This may be partially due to the fact that grid independence has

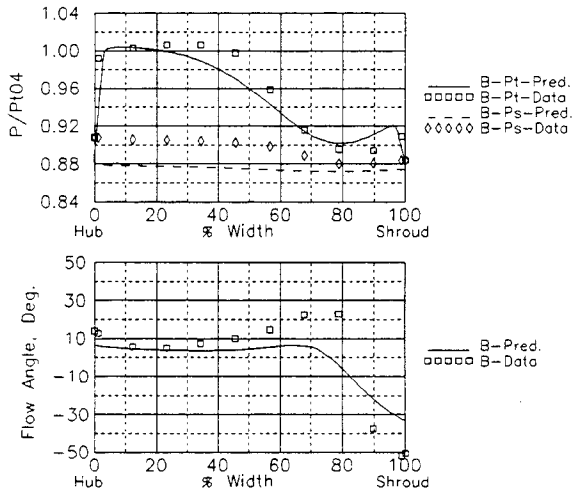

FIGURE 15. TRAVERSE B - CONFIGURATION A

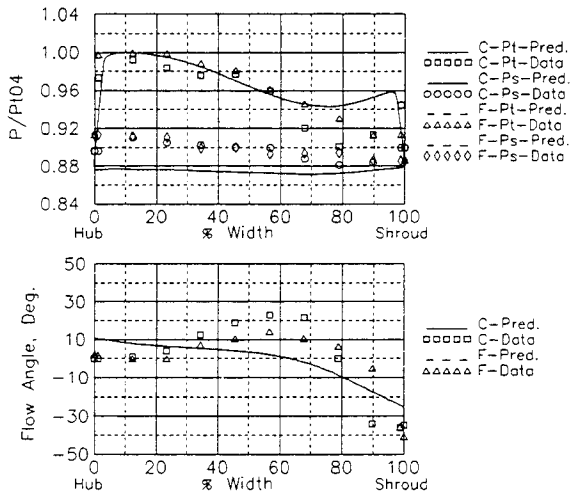

FIGURE 16. TRAVERSE C & F - CONFIGURATION A

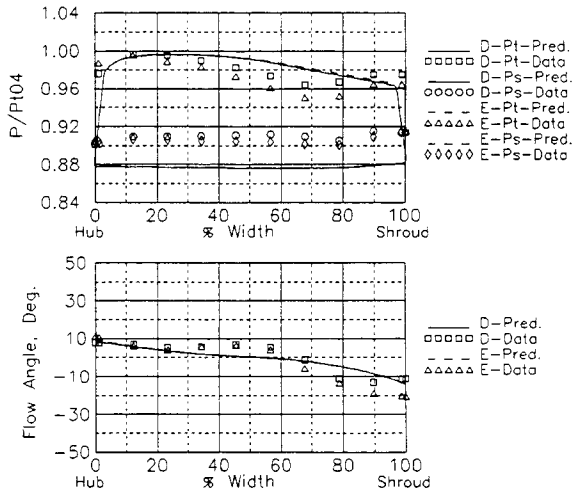

FIGURE 17. TRAVERSE D & E - CONFIGURATION A

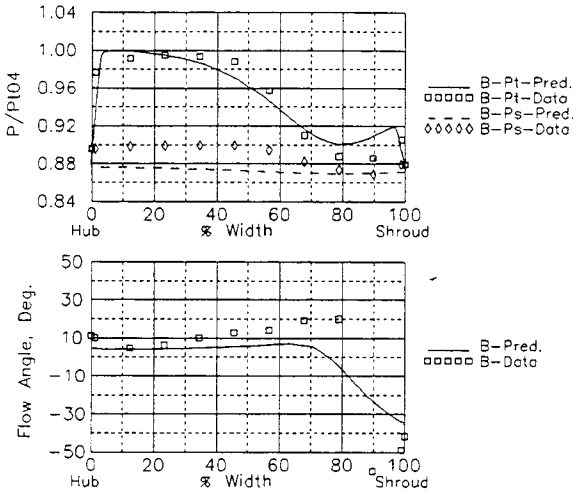

FIGURE 18. TRAVERSE B - CONFIGURATION B

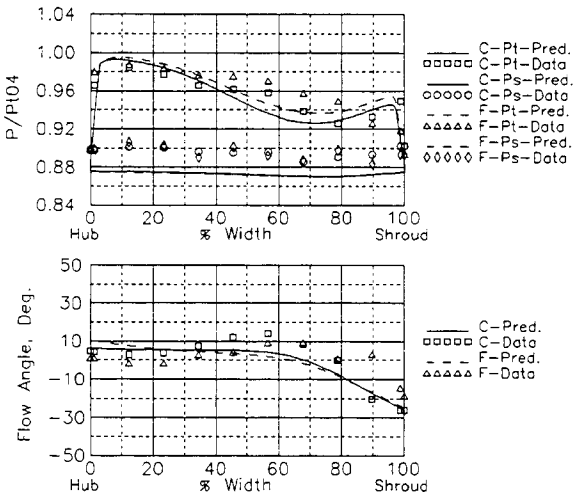

FIGURE 19. TRAVERSE C & F - CONFIGURATION B

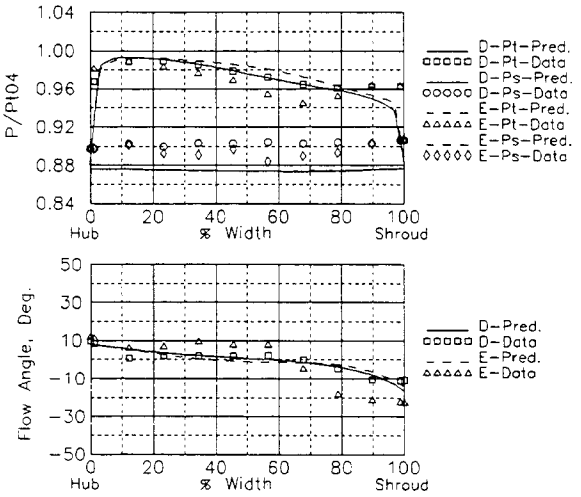

FIGURE 20. TRAVERSE D & E - CONFIGURATION B

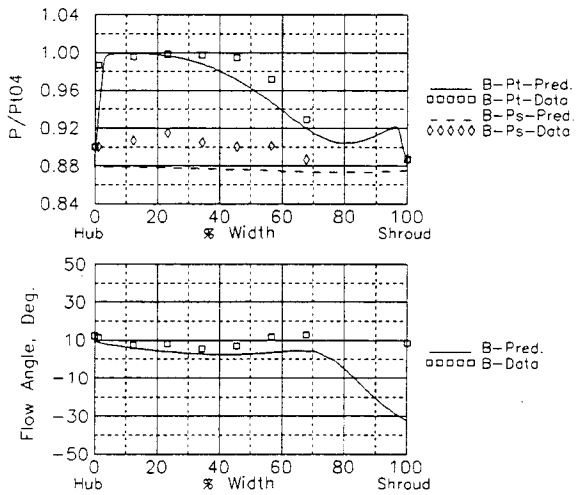

FIGURE 21. TRAVERSE B - CONFIGURATION C

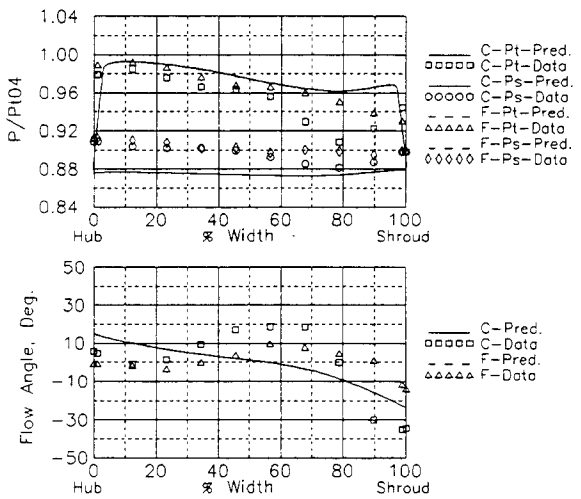

FIGURE 22. TRAVERSE C & F - CONFIGURATION C

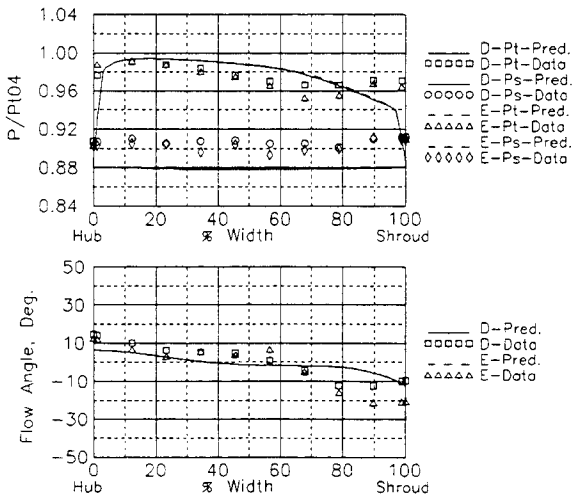

FIGURE 23. TRAVERSE D & E - CONFIGURATION C

not yet been reached for the computation, resulting in smearing of local flow features. It is also possible that the flow is not symmetric on the left and right sides of the flow for configuration A.

The data comparison for configuration B is shown in Figures 18-20. Again the experimental and computational data agree very well. It was expected that the comparison of the downstream conditions would show close agreement since the CFD prediction shows the profile distortion from the elbow is mixed out in the plenum.

Figures 21-23 show the data comparison for configuration C. Once again there is close agreement between the experimental and computational data. The downstream results for configuration C are similar to A and B, as shown in the computational study.

For all configurations, tufts located downstream of the inlet bellmouth verified the flow into the model was smooth, with no swirl. The recirculation regions in the plenum predicted by the computational study were evident from tufts placed along the plenum walls and plenum splitter vanes. Additionally, tufts placed along the guide vane walls verified the existence and location of separated flow in the guide vane passages.

It is worth noting that the computational results represent steady state solutions. However, during testing the inlet model would vibrate for all configurations at inlet Mach numbers of 0.13 and higher. This vibration would increase as the pipe inlet Mach number was increased. This unsteady behavior could be seen in the measured wall static pressure downstream of the guide vanes along the shroud wall, and in the traverse probes B, C and F at radial locations near the shroud wall. The unsteady behavior caused the traverse measured pressures to fluctuate as much as 1% of the pipe inlet total pressure.

CONCLUSIONS

The comparison of experimental and computational results shows good agreement, even within large regions of separation. The experimental and computational results confirm several locations where design modifications could improve the performance of the inlet, i.e. separation regions in the plenum, high velocities along the shroud, and separation regions due to high incidence on the guide vanes.

The computational results show that the losses in the inlet are a function of Mach number and that general flow patterns in the inlet are independent of Mach number. Results of configurations with an elbow upstream of the inlet show that flow distortion from the elbow mixes out in the plenum. The addition of the elbow does increase the losses slightly and changes the flow characteristics in the plenum, but does very little to change the exit profile of the inlet. The addition of the elbow is most detrimental when the inlet profile is not symmetrical between the two sides of the plenum (Configuration B).

Based on the results of this study, and previous CFD work on radial inlets, it is felt that CFD can be used with confidence to analyze, modify, and redesign radial inlets. The unsteady effects observed during testing demonstrate that a steady-state CFD prediction doesn't show everything. Therefore, engineering judgment must be used when reviewing CFD results to ensure the predicted solution matches the actual flow.

ACKNOWLEDGMENTS

The authors wish to acknowledge Concepts ETI for the exceptional experimental work and their attention to detail. Additionally we want to thank Dresser-Rand for allowing publication of this work.

REFERENCES

Flathers, M.B., Bache, G.E., and Rainsberger, R., 1994, "An Experimental and Computational Investigation of Flow in a Radial Inlet of an Industrial Pipeline Centrifugal Compressor," ASME Paper No. 94-GT-134.

Galpin, P.F., Huget, R.G., and Raithby, G.D., 1986, "Fluid Flow Simulations in Complex Geometries," Paper presented at the CNS/ANS Conference on Simulation Methods in Nuclear Engineering, Montreal.

Hutchinson, B.R., and Raithby, G.D., 1986, "A Multigrid Method Based on the Additive Correction Strategy," Numerical Heat Transfer, Vol. 9, pp. 511-537.

Hutchinson, B.R., Galpin, P.F., and Raithby, G.D., 1998, "Application of Additive Correction Multigrid to the Coupled Fluid Flow Equations," Numerical Heat Transfer, Vol. 13, pp. 133-147.

Raw, M., 1994, "Coupled Algebraic Multigrid for the Solution of the Discretized 3D Navier-Stokes Equations". Proceedings of the Second Annual Conference of the CFD society of Canada, Toronto, Ontario, Canada.

Schneider, G.E., and Raw, M.J., 1986, "A Skewed, Positive Influence Coefficient Upwind Procedure for Control Volume-Based Element Convection-Diffusion Computations," Numerical Heat Transfer, Vol. 8, pp. 1-26.

"TASCflow Theory Documentation", Ver. 2.3.1, March 1994, Advanced Scientific Computing.

Van Doormaal, J.P., Turan, A., and Raithby, G.D., 1987, "Evaluation of New Techniques for the Calculation of Internal Recirculating Flows," AIAA paper No. 87-0059, 25th Aerospace Sciences Meeting, Reno.

Van Doormaal, J.P., Hutchinson, B.R., and Turan, A., 1986, "An Evaluation of Techniques Used to Accelerate Segregated Methods for Predicting Viscous Fluid Flow," AIAA Paper No. 86-1653, presented at AIAA/ASME/SAE/ASEE 2nd Joint Propulsion Conference, Huntsville, Alabama.